nature genetics

Phosphoglycerate dehydrogenase diverts glycolytic flux and contributes to oncogenesis

Jason W Locasale[1,2], Alexandra R Grassian[3], Tamar Melman[1,2], Costas A Lyssiotis[1,2], Katherine R Mattaini[4], Adam J Bass[5,6], Gregory Heffron[7], Christian M Metallo[8], Taru Muranen[3], Hadar Sharfi[1,2], Atsuo T Sasaki[1,2], Dimitrios Anastasiou[1,2], Edouard Mullarky[1,2], Natalie I Vokes[4], Mika Sasaki[1,2], Rameen Beroukhim[5,6,9], Gregory Stephanopoulos[8], Azra H Ligon[5,10], Matthew Meyerson[5,6,11], Andrea L Richardson[5,10], Lynda Chin[5,12], Gerhard Wagner[7], John M Asara[2], Joan S Brugge[3], Lewis C Cantley[1,2] & Matthew G Vander Heiden[4,5]

Most tumors exhibit increased glucose metabolism to lactate, however, the extent to which glucose-derived metabolic fluxes are used for alternative processes is poorly understood[1,2]. Using a metabolomics approach with isotope labeling, we found that in some cancer cells a relatively large amount of glycolytic carbon is diverted into serine and glycine metabolism through phosphoglycerate dehydrogenase (PHGDH). An analysis of human cancers showed that *PHGDH* is recurrently amplified in a genomic region of focal copy number gain most commonly found in melanoma. Decreasing PHGDH expression impaired proliferation in amplified cell lines. Increased expression was also associated with breast cancer subtypes, and ectopic expression of PHGDH in mammary epithelial cells disrupted acinar morphogenesis and induced other phenotypic alterations that may predispose cells to transformation. Our findings show that the diversion of glycolytic flux into a specific alternate pathway can be selected during tumor development and may contribute to the pathogenesis of human cancer.

Despite the nearly universal alterations in glucose metabolism observed in tumors[1–3], it is not clear whether utilization of specific alternative pathways derived from glucose is necessary for cancer cell proliferation or whether differences in pathway fluxes contribute to the development of cancer. Metabolomics in conjunction with stable isotope labeling could allow for an unbiased interrogation of the pathways originating from glucose metabolism. To better understand the diversity of glucose metabolism, we used sensitivity-enhanced nuclear magnetic resonance (NMR)-based two-dimensional heteronuclear single quantum correlation spectroscopy (HSQC) to quantify steady-state levels of glucose-derived metabolites in HEK293T cells following 24 h of labeling with [U-^{13}C] glucose[4]. We discretized the spectra and computed the intensities of each resulting bin (**Fig. 1a** and **Supplementary Table 1**). Consistent with previous descriptions of glucose metabolism in cancer cells, two of the four highest intensity bins contained lactate peaks (**Fig. 1a**). Notably, a bin containing ^{13}C glycine was nearly as abundant as those containing ^{13}C lactate (**Fig. 1a**). To determine whether this result was general to all cultured cells[5–7], we considered two other cell lines: H1299 (an epithelial lung cancer cell line) and MCF-10A (a non-tumorigenic mammary epithelial cell line). In H1299 cells, we detected smaller relative quantities of ^{13}C-labeled glycine (**Fig. 1b**), whereas in MCF-10A cells, we observed no ^{13}C-labeled glycine (**Fig. 1b**). Together, these data indicate that cell lines have variability in glucose metabolism with differences in the relative flux of glucose to glycine.

Glycine can be generated from glucose through diversion of the glycolytic intermediate 3-phosphoglycerate (3PG) into the serine synthesis pathway and by the ultimate conversion of serine to glycine (**Fig. 1c**)[8]. The first committed step in this pathway is the oxidation of 3PG to 3-phosphohydroxypyruvate (pPYR) by the enzyme PHGDH[9]. pPYR is transaminated by phosphoserine aminotransferase (PSAT) with glutamate as a nitrogen donor to form phosphoserine (pSER) and alpha-ketoglutarate (αKG), and pSER is then dephosphorylated by phosphoserine phosphatase (PSPH) to form serine (**Fig. 1c**). Serine can be directly converted to glycine by donation of a carbon into the folate pool. This pathway defines a branching point for 3PG from glycolysis, initialized by the enzymatic activity of PHGDH, which could otherwise be metabolized to pyruvate, alanine and lactate. Flux into this pathway has been observed in cancer cells, but its cancer context, stoichiometry, requirement for cell growth and potential to promote cell transformation have not been addressed[5–7].

[1]Department of Systems Biology, Harvard Medical School, Boston, Massachusetts, USA. [2]Division of Signal Transduction, Beth Israel Deaconess Medical Center, Boston, Massachusetts, USA. [3]Department of Cell Biology, Harvard Medical School, Boston, Massachusetts, USA. [4]Koch Institute for Integrative Cancer Research, Department of Biology, Massachusetts Institute of Technology, Cambridge, Massachusetts, USA. [5]Department of Medical Oncology, Dana-Farber Cancer Institute, Harvard Medical School, Boston, Massachusetts, USA. [6]Cancer Program, Broad Institute of MIT and Harvard, Cambridge, Massachusetts, USA. [7]Department of Biochemistry and Molecular Pharmacology, Harvard Medical School, Boston, Massachusetts, USA. [8]Department of Chemical Engineering, Massachusetts Institute of Technology, Cambridge, Massachusetts, USA. [9]Department of Cancer Biology, Dana-Farber Cancer Institute, Harvard Medical School, Boston, Massachusetts, USA. [10]Department of Pathology, Brigham and Women's Hospital, Boston, Massachusetts, USA. [11]Center for Cancer Genome Discovery, Dana-Farber Cancer Institute, Harvard Medical School, Boston, Massachusetts, USA. [12]Department of Dermatology, Harvard Medical School, Boston, Massachusetts, USA. Correspondence should be addressed to J.W.L. (jlocasal@bidmc.harvard.edu), M.G.V.H. (mvh@mit.edu) or L.C.C. (lcantley@hms.harvard.edu).

Received 19 July 2010; accepted 27 June 2011; published online 31 July 2011; doi:10.1038/ng.890

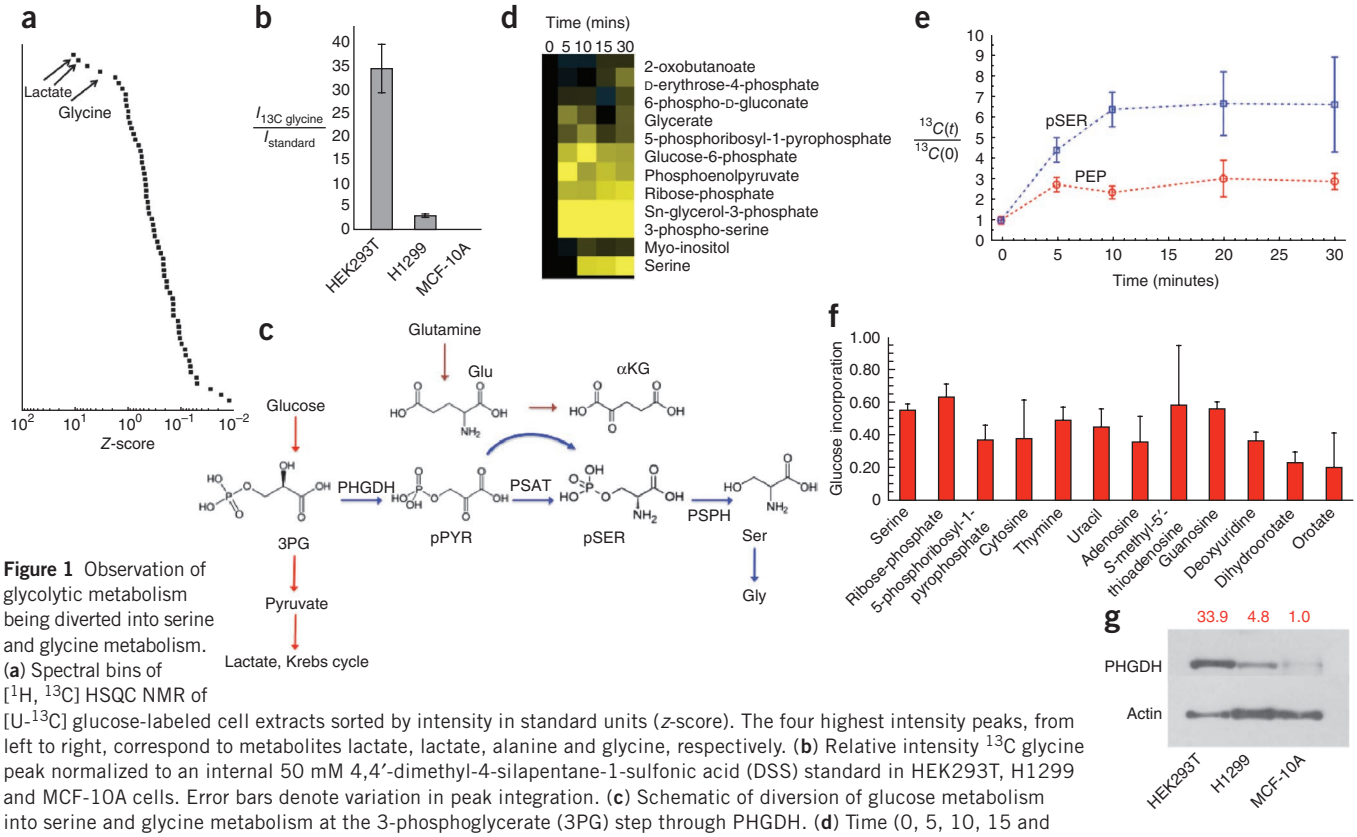

Figure 1 Observation of glycolytic metabolism being diverted into serine and glycine metabolism. (**a**) Spectral bins of [^{1}H, ^{13}C] HSQC NMR of [U-^{13}C] glucose-labeled cell extracts sorted by intensity in standard units (*z*-score). The four highest intensity peaks, from left to right, correspond to metabolites lactate, lactate, alanine and glycine, respectively. (**b**) Relative intensity ^{13}C glycine peak normalized to an internal 50 mM 4,4′-dimethyl-4-silapentane-1-sulfonic acid (DSS) standard in HEK293T, H1299 and MCF-10A cells. Error bars denote variation in peak integration. (**c**) Schematic of diversion of glucose metabolism into serine and glycine metabolism at the 3-phosphoglycerate (3PG) step through PHGDH. (**d**) Time (0, 5, 10, 15 and 30 min) courses of U-^{13}C labeling intensities of 12 metabolites from [U-^{13}C] glucose labeling experiments measured with targeted LC/MS/MS relative to baseline level at time 0. (**e**) Comparison of 3-phosphoserine (pSER) and phosphoenolpyruvate (PEP) labeling kinetics of [U-^{13}C] glucose relative to baseline level at time 0 with targeted LC/MS/MS. Error bars represent the s.d. of three biological replicates. (**f**) Relative glucose flux into serine biosynthesis measured by steady-state labeling of [U-^{13}C] glucose into serine with targeted LC/MS/MS. The fraction of labeled to unlabeled glucose-derived metabolites, ^{13}C/(^{12}C + ^{13}C) ion intensities (glucose incorporation), is plotted for 12 metabolites. Serine is compared with respect to the glucose-labeled fraction of downstream nucleotides and other nucleotide precursors. Error bars represent the s.d. of three biological replicates. (**g**) Relative protein levels (as determined by protein blot analysis) of PHGDH in HEK293T, H1299 and MCF-10A cells with a β-actin (actin) loading control shown below the PHGDH band. Quantitation relative to the levels in MCF-10a cells of the total intensity of the PHGDH band relative to the actin band is shown above.

To further interrogate glucose metabolism, we monitored the time course of conversion of [U-^{13}C] glucose to other metabolites using targeted liquid chromatography mass spectrometry (LC/MS/MS)[10] in HEK293T cells. We detected ^{13}C-labeled glucose incorporation into 13 metabolites, in multiple pathways, over the 30-min time course (**Fig. 1d**). The time required for labeled carbon to reach steady state in a pathway is a measurement of pathway flux. The data in **Figure 1e** show that ^{13}C incorporation into pSER (^{13}C-pSER) reaches steady state at a time scale comparable to the time for phosphoenolpyruvate (PEP) to reach steady state, suggesting that the relative fluxes are comparable. The ^{13}C-pSER labeling accompanied labeling of serine (**Supplementary Fig. 1a**), and labeling of serine was also confirmed using gas chromatography mass spectrometry (GC/MS) by measuring pool sizes of incorporation of [α-^{15}N] glutamine into amino acids (**Supplementary Fig. 1b**). These data are in agreement with our NMR experiments, suggesting that a substantial fraction of glucose is diverted from 3PG into the serine and glycine biosynthetic pathway in these cells. To measure the total amount of glucose-derived serine, we cultured HEK293T cells in uniformly labeled ^{13}C glucose and measured metabolites from cell extracts using LC/MS/MS. We found the amount of labeled serine to be about one half of the total serine, and this value was commensurate with the relative amount of glucose incorporation into nucleotides and nucleotide intermediates (**Fig. 1f**). Differences in PHGDH protein expression in the three cell lines corresponded to differences in the amount of glycine synthesized from glucose (**Fig. 1g**).

The specific diversion of glucose metabolism through PHGDH suggested a possible context in which selective pressure exists for tumors to increase PHGDH activity. One mechanism that can enhance PHGDH activity is an increase in the copy number at the genomic locus containing *PHGDH*. We identified *PHGDH* as a frequently amplified gene in a pooled analysis of somatic copy number alterations across 3,131 cancer samples[11]. We found *PHGDH* in a peak region at chromosome 1p12 that shows recurring copy number gain in 16% of all cancers (**Supplementary Table 2**). No known oncogenes are contained in the peak region of five genes (*PHGDH*, *REG4*, *HMGCS2*, *NBPF7* and *ADAM30*) at this locus. *PHGDH* is located in one of four peak regions of chromosome 1p ($q = 1.12 \times 10^{-9}$) (**Fig. 2a**, left). Two of the three high-scoring peaks contain the oncogenes *MYCL1* at 1p34 ($q = 1.7 \times 10^{-14}$) and *JUN* at 1p32 ($q = 8.55 \times 10^{-7}$) (**Fig. 2a**, left). We plotted the copy number intensity of 150 cancers sorted by highest *PHGDH* copy number (**Fig. 2a**, middle) along chromosome 1p; that plot showed that most samples containing *PHGDH* copy number gain have the genomic amplification localized near the 1p12 region. An inspection of the genomic region containing *PHGDH* (**Fig. 2a**, right) showed the localized amplification within the coding region of *PHGDH*. Amplification was found most commonly in melanoma (**Supplementary Fig. 2**)

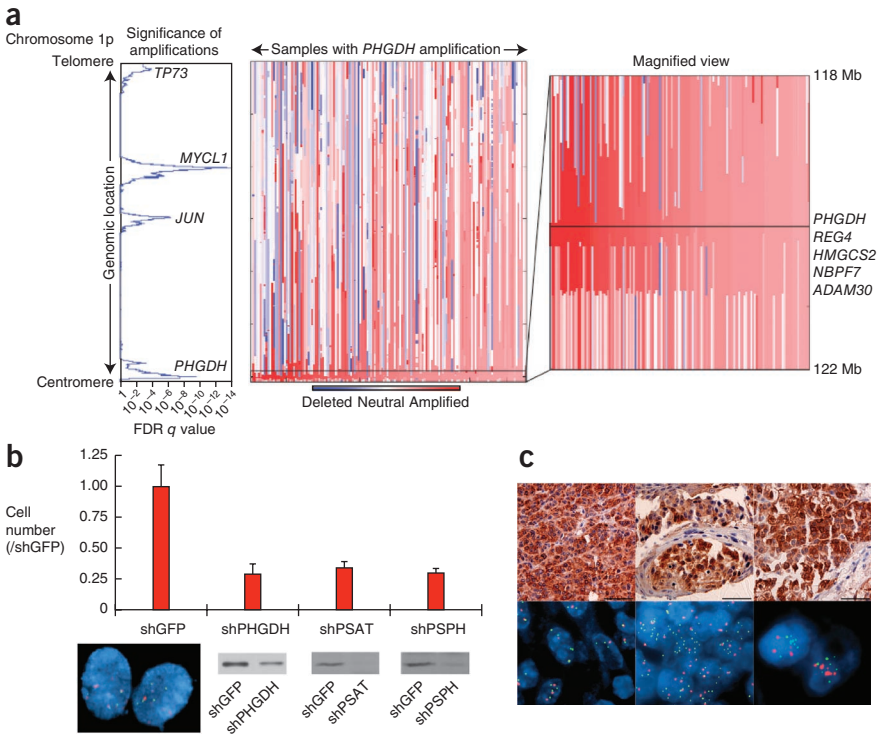

Figure 2 *PHGDH* amplification in human cancers and requirement for proliferation. (**a**) *PHGDH* copy number intensity across 3,131 cancer samples. The left plot shows the significance of the amplifications (false discovery rate (FDR) *q* value) along chromosome 1p (from telomere to centromere). Candidate oncogenes (*TP73*, *MYCL1* and *JUN*) in three peak regions and corresponding FDR *q* values are shown. The FDR *q* value of *PHGDH* is shown in the fourth peak region. The middle plot shows the copy number intensity along chromosome 1p of 150 cancers containing the highest intensity of *PHGDH* amplification, illustrating the localized intensity near the region of *PHGDH*. The right plot shows magnification of the 4-Mb region containing *PHGDH*. The solid line indicates the chromosome position of the *PHGDH* coding region. (**b**) Relative cell numbers of T.T. cells upon knockdown with shGFP, shPHGDH, shPSAT and shPSPH relative to an shRNA directed against GFP. Error bars represent the s.d. of three independent measurements. Shown below is an interphase FISH analysis showing *PHGDH* copy number gain in T.T. cells. The green probe maps to 1p12 and includes the *PHGDH* coding sequence. The red probe maps to the pericentromeric region of chromosome 1 (1p11.2–q11.1). FISH images were taken at 100× power. Also shown below are relative protein levels of PHGDH, PSAT and PSPH (as determined by protein blot analysis). (**c**) PHGDH protein expression and copy number gain in three representative human melanoma tissue samples. In the upper panels, we assessed PHGDH expression in tumor samples using immunohistochemistry (IHC). Nuclei are shown in blue (hematoxylin), and PHGDH antibody staining is shown in brown (3-3′-diaminobenzidine (DAB)). Scale bars, 50 μm. The lower panels show interphase FISH analysis carried out as in **b** in matched samples to assess copy number. FISH images were taken at 100× power.

at 40% frequency in a three-gene peak region ($q = 1.93 \times 10^{-5}$), with *HMGCS2* and *REG4* also contained in the peak.

We first examined T.T. cells, an esophageal squamous cell carcinoma cell line that contains a highly focal copy number gain of *PHGDH* (ref. 11) as determined by SNP array, and carried out fluorescence *in situ* hybridization (FISH) to verify copy number gain (**Fig. 2b**). Focal copy number gain in *PHGDH* suggested that its expression might be important for proliferation in these cells, and stable knockdown of PHGDH (or the downstream enzymes PSAT and PSPH) reduced proliferation (**Fig. 2b**).

Because we found *PHGDH* amplification most commonly in melanoma, we assessed PHGDH expression and copy number gain in human melanoma tissue samples. We observed high PHGDH protein expression (immunohistochemistry (IHC) score > 1) in 21% of the samples (**Supplementary Fig. 3a**,**b**). We observed *PHGDH* copy number gain using FISH in 21 of 42 samples (**Supplementary Fig. 3c**), however, 16 of these samples also contained an equal increased copy number of a probe sequence adjacent to the centromere, indicating either polysomy or amplification of the pericentromeric region of chromosome 1p. Five tumors had copy number gain relative to the number of pericentromeric probes (**Fig. 2c**). Each of these samples had high expression shown by IHC (**Fig. 2c**), indicating that *PHGDH* copy number gain associates with significant protein overexpression in human melanoma ($P = 0.0045$, Fisher's exact test, two-tailed).

We next investigated whether melanoma cell lines containing *PHGDH* copy number gain would be sensitive to decreased expression of PHGDH. We obtained three tumor-derived human melanoma cell lines (WM1266-3, Malme-3M and Sk-Mel28) with 1p12 gain, along with two additional melanoma cell lines (Gak and Carney)[12]. For each cell line, we created pairs of cell lines containing short hairpin RNA (shRNA) targeting PHGDH or targeting GFP as a control (**Fig. 3a**, left). Each of the amplified cell lines showed decreased proliferation relative to the non-amplified cell lines upon PHGDH knockdown, indicating that the growth of the amplified cell lines is differentially sensitive to PHGDH knockdown (**Fig. 3a**, right). To verify that high expression leads to increased flux through the serine pathway, we measured the relative incorporation of ^{13}C serine from [U-^{13}C] glucose and found that each of the amplified cell lines had appreciable serine labeling from glucose (**Fig. 3b**). One cell line that did not contain the amplification (Carney) had high expression of PHGDH and high flux into serine synthesis (**Fig. 3a**,**b**). Previous studies of oncogene addiction have shown that loss of cancer-cell proliferation correlates with the presence of a genetic lesion and not with gene expression[13,14]. Consistent with these findings, we observed that PHGDH knockdown had no effect on proliferation in Carney cells despite increased serine pathway flux (**Fig. 3a**).

We then asked whether knockdown of PHGDH to levels that impair proliferation affects metabolism. We measured metabolite levels in Sk-Mel28 cells using targeted LC/MS/MS to profile metabolite levels with or without knockdown of PHGDH. PHGDH knockdown reduced pSER levels in Sk-Mel28 cells (**Fig. 3c**) and globally altered the levels of many metabolites, including many intermediates in glycolysis (**Fig. 3d** and **Supplementary Table 3**). We observed increased levels of metabolites in glycolysis near the point of diversion into serine metabolism (**Fig. 3e**), confirming that the level of PHGDH expression alters glucose metabolism in Sk-Mel28 cells by modulating the entry of glycolytic metabolites into serine metabolism.

Recently, high *PHGDH* mRNA expression was found to be associated with poor prognosis in breast cancer[15]. To further investigate the role of *PHGDH* in this disease, we carried out a meta-analysis of

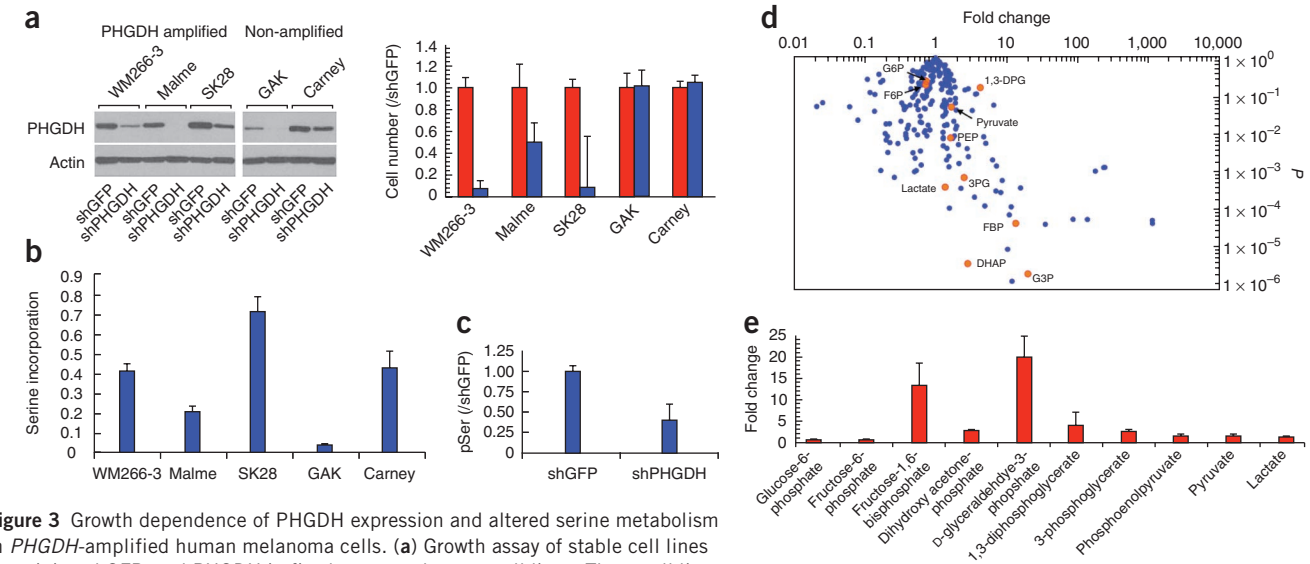

Figure 3 Growth dependence of PHGDH expression and altered serine metabolism in *PHGDH*-amplified human melanoma cells. (**a**) Growth assay of stable cell lines containing shGFP or shPHGDH in five human melanoma cell lines. Three cell lines (WM266-3, Malme-3M (Malme) and Sk-Mel28 (SK28)) contain 1p12 copy number gain; two other melanoma cell lines (GAK and Carney) were also considered. The left panel shows a protein blot analysis of protein levels of PHGDH, and the corresponding protein levels of actin are shown as a loading control. On the right, the cell numbers for shGFP and shPHGDH normalized to shGFP are plotted for each cell line. Error bars represent the s.d. of three independent measurements. (**b**) Relative amount of glucose flux into serine biosynthesis measured by steady-state labeling of [U-^{13}C] glucose into serine with targeted LC/MS/MS. The fraction of labeled to unlabeled glucose-derived serine to total serine, $^{13}C/(^{12}C + ^{13}C)$ (serine incorporation), is measured in each of the five cell lines. Error bars represent the s.d. of three independent measurements. (**c**) Relative ion intensities of 3-phosphoserine (pSer) in control (shGFP) and knockdown (shPHGDH) cells normalized to intensity in knockdown shGFP cells (pSer/shGFP). Error bars represent the s.d. of three independent measurements. (**d**) Scatter plot of the ratio of intensities (fold change) versus *P* value (Student's *t*-test) of shPHGDH relative to shGFP in Sk-Mel28 cells. (**e**) Ratio of intensities (fold change) of glycolytic intermediates upon PHGDH knockdown (shPHGDH) relative to (shGFP) in Sk-Mel28 cells. Error bars represent the propagation of error of the s.d. from three independent measurements.

tumor microarray data and found strong associations ($P < 1 \times 10^{-4}$) with several clinical parameters in breast cancer (**Supplementary Fig. 4** and **Supplementary Table 4**). These data suggest that *PHGDH* expression segregated with specific cancer subtypes. For validation, we assessed PHGDH protein expression in 106 human breast cancer tumor samples using IHC (**Supplementary Fig. 5a**) and correlated protein levels with mRNA expression (**Supplementary Fig. 5b**). We found that high PHGDH expression (IHC score > 1) was associated with specific breast cancer subsets, as expression correlated with both triple-negative[16] ($P = 0.002$, Fisher's exact, two tailed) and basal subtypes ($P = 0.004$, Fisher's exact, two tailed) (**Supplementary Fig. 6**). However, there was no association with general parameters such as metastasis, as was previously reported[15], or with tumor size, suggesting that expression is subtype specific. Consistent with a reliance of a subset of breast cancers on PHGDH, protein expression was required for growth in a panel of three (BT-20, SK-BR-3 and MCF-7) breast cancer cell lines to differing extents (including the BT-20 cell line that carries *PHGDH* amplification) (**Supplementary Fig. 7a**). In contrast, non-tumorigenic breast epithelial cells (MCF-10A) did not require PHGDH for growth (**Supplementary Fig. 7a**), did not show alterations in glycolysis upon shRNA knockdown of PHGDH (**Supplementary Fig. 7b**) and showed no detectable labeling of pSER from glucose (**Supplementary Fig. 7c**).

We therefore asked whether ectopic expression of PHGDH would increase the flux of glucose to serine and result in any phenotypic consequences. MCF-10A cells are non-tumorigenic and when grown in reconstituted basement membrane (Matrigel) form structures resembling many features of mammary acini. This model has been used to monitor alterations in growth arrest, polarization, invasive behavior and other disruptions of normal morphogenesis that resemble changes associated with different stages of tumor formation[17]. We introduced PHGDH into MCF-10A cells using a tetracycline-inducible vector, and increasing concentrations of doxycycline increased expression of PHGDH (**Fig. 4a**). pSER levels were elevated to detectable levels in cells treated with 1 μg/ml doxycycline, indicating an increase in pathway activity (**Fig. 4b**) that was confirmed by an increase in serine and glycine synthesis (**Supplementary Fig. 7d**).

We seeded PHGDH-expressing MCF-10A cells in Matrigel reconstituted basement membrane and monitored the structures at increasing doses of doxycycline using confocal microscopy and immunofluorescence staining of nuclei (4′,6-diamidino-2-phenylindole (DAPI)) and extracellular matrix (laminin-5) (**Fig. 4c**). In the absence of doxycycline, MCF-10A cells formed hollow, acini-like structures, as previously reported[18] (**Fig. 4c**). In contrast, PHGDH-expressing cells formed disorganized structures lacking a lumen (**Fig. 4c**). The PHGDH-expressing cells also had large, abnormal nuclear morphologies, failed to orient in a uniform fashion adjacent to the basal acinar membrane and showed enhanced proliferation (**Fig. 4d**). The majority of the control acini were either clear or mostly clear, whereas PHGDH expression dramatically increased the percentage of acini that scored as mostly filled or filled in a dose-dependent manner (**Fig. 4e**). A hypomorphic mutant PHGDH (p.Val490Met)[19] showed decreased luminal filling (**Fig. 4f** and **Supplementary Fig. 7e**). In addition, MCF-10A acini with ectopic expression of wild-type but not mutant PHGDH showed mislocalization of the Golgi apparatus, indicating loss of apical polarity (**Fig. 4f**). These results indicate that PHGDH expression alters glucose metabolism, disrupts luminal organization and polarity and preserves the viability of the matrix-deprived cells to survive in an anchorage-independent fashion. Notably, these phenotypes depend on the catalytic activity of PHGDH.

Although numerous studies have correlated oncogenesis with changes in cell metabolism, only a few studies have suggested that

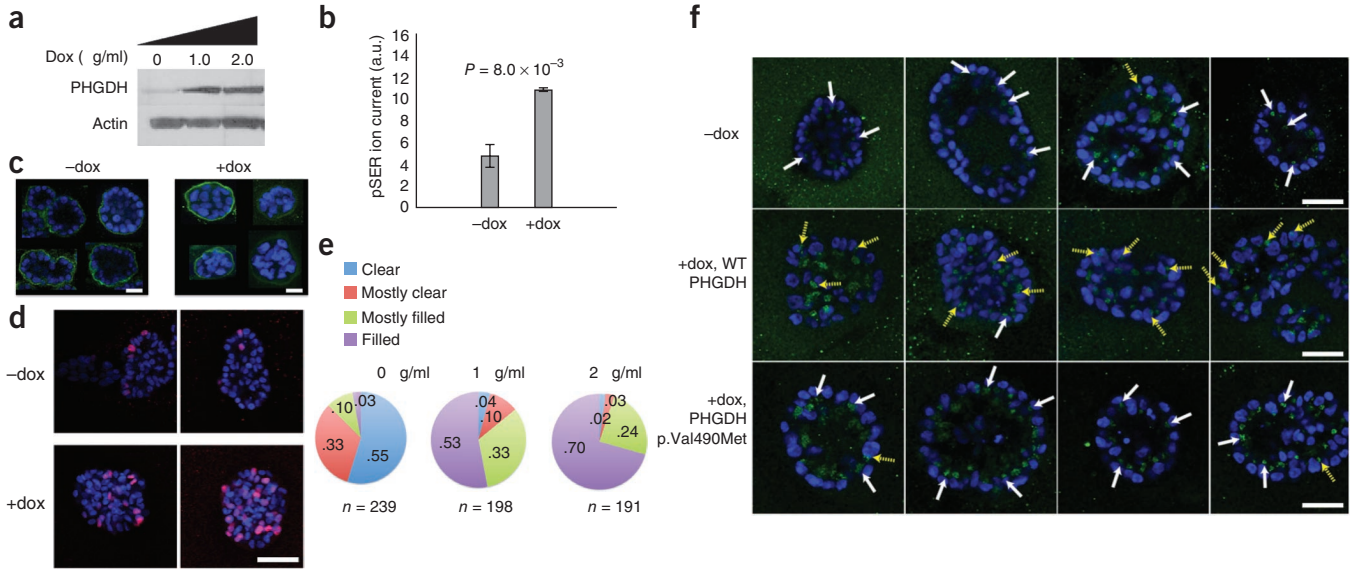

Figure 4 Ectopic expression of PHGDH in breast ductal morphogenesis. (**a**) Protein expression of PHGDH by protein blot analysis, with actin as loading control for three concentrations of doxycycline (dox) (0 μg/ml, 1 μg/ml and 2 μg/ml). (**b**) pSER integrated intensities in –dox (0 μg/ml) and +dox (1 μg/ml) (a.u., arbitrary units). Error bars represent the s.d. of three independent measurements. (**c**) Confocal images of DAPI (blue) and laminin-5 (green). Representative images from four acini from MCF-10A cells expressing doxycyline-inducible PHGDH without doxycycline (–dox) or 1 μg/ml doxycyline (+dox). Scale bars, 50 μm. (**d**) Enhanced proliferation in the interior of PHGDH-expressing acini. Representative images from acini from MCF-10A cells expressing doxycyline-inducible PHGDH without doxycycline (–dox) or 1 μg/ml doxycyline (+dox). Confocal images of MCF-10A cells under the same conditions as in **c** with DAPI (blue) and the proliferation marker Ki67 (red). Scale bar, 50 μm. (**e**) Quantification of acinar filling for 0 μg/ml, 1 μg/ml and 2 μg/ml dox. Each acinus was scored as filled, mostly filled, mostly clear or clear. Data are representative of multiple independent measurements. (**f**) Loss of apical polarity in PHGDH-expressing cells. Confocal images of MCF-10A cells under the same conditions as in **c** with DAPI (blue) and Golgi apparatus (green). Solid white arrows indicate cells with an oriented Golgi apparatus. Dashed yellow arrows indicate cells with loss of polarity. Acini with ectopic expression of wild-type (WT) PHGDH, but not mutant p.Val490Met PHGDH, commonly display a mislocalized Golgi apparatus, indicative of a lack of cell polarity. Scale bars, 50 μm; –dox, 0 μg/ml; +dox, 1 μg/ml.

genetic aberrations in metabolic genes are capable of driving tumorigenesis[20]. Here we show that PHGDH, a focus of recurrent genomic amplification, diverts glucose-derived carbon into a specific biosynthetic pathway and that this change in metabolism can be selected for in the development of human cancer. The diversion of glycolytic flux into *de novo* serine biosynthesis has a multitude of biological consequences. Pathways downstream of serine metabolism contribute to biosynthesis and metabolic signaling functions associated with the folate pool, amino acid and lipid intermediates, and redox regulation[18,21–23]. In addition, the process of diverting fluxes from 3PG out of glycolysis confers several advantages for cell growth. These include limiting ATP production, oxidation of 3PG to influence redox status and the generation of αKG from glutamate, all of which are reported to benefit cell growth through multiple mechanisms[24–26]. As the consequences of *PHGDH* amplification and increased glucose flux into serine metabolism are multi-factorial, it is not likely that a single isolated mechanism leads to cell transformation downstream of *PHGDH* amplification. Nevertheless, the observation that a genetic lesion can function to directly alter metabolic flux out of glycolysis provides avenues for further inquiry and shows that alterations in metabolism beyond increased lactate production are important events in the development of cancer.

URLs. ImageJ software, http://rsbweb.nih.gov/ij/; NMRPipe, http://spin.niddk.nih.gov/NMRPipe/; MATLAB, http://www.mathworks.com/products/matlab/; Sparky software package, http://www.cgl.ucsf.edu/home/sparky/; protocol for generating acini cells, http://brugge.med.harvard.edu/; CHORI, http://www.chori.org/; Oncomine, https://www.oncomine.org/resource/login.html.

METHODS

Methods and any associated references are available in the online version of the paper at http://www.nature.com/naturegenetics/.

Note: Supplementary information is available on the Nature Genetics website.

ACKNOWLEDGMENTS

Microscopy data for this study were acquired and analyzed in the Nikon Imaging Center at Harvard Medical School. J.W.L. was supported by postdoctoral fellowships from the US National Institutes of Health (NIH) and the American Cancer Society. A.R.G. is a recipient of a National Science Foundation (NSF) Graduate Research Fellowship. L.C.C. and J.S.B. were supported by grants from the NIH and the National Cancer Institute (NCI). M.G.V.H. was supported by grants from the NIH, NCI, Smith Family, Damon Runyon Cancer Research Foundation and the Burroughs Wellcome Fund. We thank N. Vena for technical assistance with the FISH analysis and K. Webster and I. Carrecedo for help with immunohistochemistry. We thank J. Rabinowitz, A. Carrecedo and S.-C. Ng for helpful comments on the manuscript.

AUTHOR CONTRIBUTIONS

J.W.L., M.G.V.H. and L.C.C. designed the study and wrote the paper. J.W.L., C.A.L., E.M., K.R.M., D.A., H.S., M.G.V.H. and T. Melman carried out experiments. J.W.L. and T. Melman carried out computational analyses. A.J.B., R.B. and M.M. provided help with copy number data. L.C. and A.L.R. provided human cancer samples. N.I.V. and A.H.L. carried out the FISH analysis. J.W.L. and J.M.A. carried out the LC/MS/MS experiments. J.W.L., G.H. and G.W. carried out the NMR experiments. J.W.L., N.I.V., C.M.M. and G.S. carried out the GC/MS experiments. M.S. and A.T.S. generated reagents. J.S.B., T. Muranen and A.R.G. carried out experiments involving acinar morphogenesis and imaging analysis.

COMPETING FINANCIAL INTERESTS

The authors declare competing financial interests: details accompany the full-text HTML version of the paper at http://www.nature.com/naturegenetics/.

Published online at http://www.nature.com/naturegenetics/.
Reprints and permissions information is available online at http://www.nature.com/reprints/index.html.

1. Vander Heiden, M.G., Cantley, L.C. & Thompson, C.B. Understanding the Warburg effect: the metabolic requirements of cell proliferation. *Science* **324**, 1029–1033 (2009).
2. DeBerardinis, R.J., Lum, J.J., Hatzivassiliou, G. & Thompson, C.B. The biology of cancer: metabolic reprogramming fuels cell growth and proliferation. *Cell Metab.* **7**, 11–20 (2008).
3. Warburg, O., Posener, K. & Negelein, E. Ueber den Stoffwechsel der Tumoren. *Biochem. Z.* **152**, 319–344 (1924).
4. Bodenhausen, G. & Ruben, D.J. Natural abundance nitrogen-15 NMR by enhanced heteronuclear spectroscopy. *Chem. Phys. Lett.* **69**, 185–189 (1980).
5. Bismut, H., Caron, M., Coudray-Lucas, C. & Capeau, J. Glucose contribution to nucleic acid base synthesis in proliferating hepatoma cells: a glycine-biosynthesis-mediated pathway. *Biochem. J.* **308**, 761–767 (1995).
6. Snell, K., Natsumeda, Y. & Weber, G. The modulation of serine metabolism in hepatoma 3924A during different phases of cellular proliferation in culture. *Biochem. J.* **245**, 609–612 (1987).
7. Kit, S. The biosynthesis of free glycine and serine by tumors. *Cancer Res.* **15**, 715–718 (1955).
8. de Koning, T.J. *et al.* L-serine in disease and development. *Biochem. J.* **371**, 653–661 (2003).
9. Achouri, Y., Rider, M.H., Van Schaftingen, E. & Robbi, M. Cloning, sequencing and expression of rat liver 3-phosphoglycerate dehydrogenase. *Biochem. J.* **323**, 365–370 (1997).
10. Lu, W., Bennett, B.D. & Rabinowitz, J.D. Analytical strategies for LC-MS-based targeted metabolomics. *J. Chromatogr. B Analyt. Technol. Biomed. Life Sci.* **871**, 236–242 (2008).
11. Beroukhim, R. *et al.* The landscape of somatic copy-number alteration across human cancers. *Nature* **463**, 899–905 (2010).
12. Greshock, J. *et al.* A comparison of DNA copy number profiling platforms. *Cancer Res.* **67**, 10173–10180 (2007).
13. Slamon, D.J. *et al.* Human breast cancer: correlation of relapse and survival with amplification of the HER-2/neu oncogene. *Science* **235**, 177–182 (1987).
14. Luo, J., Solimini, N.L. & Elledge, S.J. Principles of cancer therapy: oncogene and non-oncogene addiction. *Cell* **136**, 823–837 (2009).
15. Pollari, S. *et al.* Enhanced serine production by bone metastatic breast cancer cells stimulates osteoclastogenesis. *Breast Cancer Res. Treat.* **125**, 421–430 (2011).
16. Foulkes, W.D., Smith, I.E. & Reis-Filho, J. Triple-negative breast cancer. *N. Engl. J. Med.* **363**, 1938–1948 (2010).
17. Debnath, J. & Brugge, J.S. Modelling glandular epithelial cancers in three-dimensional cultures. *Nat. Rev. Cancer* **5**, 675–688 (2005).
18. Schafer, Z.T. *et al.* Antioxidant and oncogene rescue of metabolic defects caused by loss of matrix attachment. *Nature* **461**, 109–113 (2009).
19. Tabatabaie, L. *et al.* Novel mutations in 3-phosphoglycerate dehydrogenase (PHGDH) are distributed throughout the protein and result in altered enzyme kinetics. *Hum. Mutat.* **30**, 749–756 (2009).
20. Thompson, C.B. Metabolic enzymes as oncogenes or tumor suppressors. *N. Engl. J. Med.* **360**, 813–815 (2009).
21. Teperino, R., Schoonjans, K. & Auwerx, J. Histone methyl transferases and demethylases: can they link metabolism and transcription? *Cell Metab.* **12**, 321–327 (2010).
22. Nomura, D.K. *et al.* Monoacylglycerol lipase regulates a fatty acid network that promotes cancer pathogenesis. *Cell* **140**, 49–61 (2010).
23. Hara, K. *et al.* Amino acid sufficiency and mTOR regulate p70 S6 kinase and eIF-4E BP1 through a common effector mechanism. *J. Biol. Chem.* **273**, 14484–14494 (1998).
24. Vander Heiden, M.G. *et al.* Evidence for an alternative glycolytic pathway in rapidly proliferating cells. *Science* **329**, 1492–1499 (2010).
25. Locasale, J.W. & Cantley, L.C. Altered metabolism in cancer. *BMC Biol.* **8**, 88 (2010).
26. Eng, C.H., Yu, K., Lucas, J., White, E. & Abraham, R.T. Ammonia derived from glutaminolysis is a diffusible regulator of autophagy. *Sci. Signal.* **3**, ra31 (2010).

ONLINE METHODS

***PHGDH* cloning.** A human *PHGDH* complementary DNA fragment was cloned into a pLvx-Tight-Puro (Clontech) tetracycline-inducible vector.

***PHGDH* RNA interference.** shRNA hairpins in the lentiviral vector plasmids pLKO.1 were purchased from Open Biosystems. The *PHGDH* targeting sequences (shPHGDH) used were CCGGAGGTGATAACACAGGGAACAT CTCGAGATGTTCCCTGTGTTATCACCTTTTTT (TRCN0000028548) and CCGGCTTAGCAAAGAGGAGCTGATACTCGAGTATCAGCTCCTCTTTG CTAAGTTTTT (TRCN0000028545). A control hairpin in the pLKO.1 vector was used that targeted *GFP* (shGFP). HEK293T cells were transfected with pLKO.1 vectors and lenti-viral packaging vectors. Selection under 2 μg/ml puromycin was carried out at least two days before experiments.

Cell lysis, protein blot and immunohistochemistry analysis. Exponentially growing cells were first washed with cold PBS and lysed with RIPA buffer (10 mM Tris (pH 7.5), 150 mM NaCl, 1% Nonidet P-40, 1% Deoxycholic acid, 0.1% SDS and 4 μg/ml each of pepstatin, leupeptin and 4-(2-aminoethyl) benzenesulfonyl fluoride hydrochloride) and aprotinin, a phosphatase inhibitor cocktail (Thermo Scientific), and 1 mM dithiothreitol (DTT). Lysates were centrifuged at 20,000*g* at 4 °C for 30 min, and the supernatant was retained. Protein concentration was determined with a Bradford assay (Bio-Rad). Mouse monoclonal PHGDH antibody was purchased from Santa Cruz (sc-100317), and mouse monoclonal β-actin (abCam ab8226) was used as a loading control. Both mouse PSAT antibody (Novus) and rabbit PSPH antibody (Sigma) were used at dilutions of 1:1,000. PHGDH antibody was used at 1:500 dilution and incubated at 4 °C overnight with 5% dry milk in Tris-buffered saline (0.05% Tween). β-actin antibody was used at a 1:10,000 dilution. Secondary antibodies conjugated to horseradish peroxidase were used at a 1:10,000 dilution. Protein blots were developed using chemiluminescence. Quantitation was carried out using ImageJ software (see URLs). For immunohistochemistry, mouse PHGDH antibody was purchased from Santa Cruz (sc-100317) and used at a 1:15 dilution. Antibody specificity was first validated using paraffin-embedded cell blocks obtained from shGFP- and shPHGDH-expressing cell lines. All IHC staining was carried out using a Dako Envision (K4006) IHC kit with hematoxylin nuclear counterstain and 3-3′-diaminobenzidine (DAB) antibody stain.

Cell culture. The T.T. cell line was a gift from A. Rustgi. All human melanoma cell lines were obtained by L.C. All other cell lines were obtained from ATCC and cultured under ATCC protocols. T.T. cells were grown with Dulbecco's Modified Eagle Medium (DMEM) (Mediatech), 10% FBS and antibiotics (penicilin/streptomycin, Invitrogen). All human melanoma cell lines were cultured as previously in Roswell Park Memorial Institute medium (RPMI) (Mediatech) with 10% FBS and antibiotics. Growth media contained the standard concentrations of glutamine but was not supplemented with additional glutamine.

NMR sample preparation, spectroscopy and data analysis. We harvested 10^8 exponentially growing HEK293T, H1299 and MCF-10a cells growing in basal growth media with dialyzed serum and extracted metabolites in 50 ml of 80% methanol (v/v) at dry ice temperatures. Cells were incubated with [U^{13}C] glucose (Cambridge Isotope Laboratories), replaced at 25 mM and incubated for 24 h before harvesting. Fresh media were added 2 h before the experiment. Lysates were centrifuged at 10,000 *g* for 30 min at 4 °C, and the supernatant was stored. Methanol was first evaporated at 15 °C under vacuum with rotational evaporation, and samples were subsequently lyophilized. Samples were prepared for NMR spectroscopy by resuspending the lyophilized material in 700 μl of sample buffer containing 50 mM $NaPO_4$, pH 7.0, and 2 mM DSS (as an internal standard and chemical shift reference).

All NMR spectra were acquired on a Bruker 500 MHz spectrometer (Bruker, Inc.) using a 5 mm triple resonance (H, C, N) Cryoprobe. The sample temperature was 25 °C for all samples. Two-dimensional ^{1}H-^{13}C HSQC spectra with sensitivity enhancement were acquired with spectral widths of 12,000 Hz and 9,048 Hz in the direct and indirect dimensions, respectively. We acquired 1,024 complex data points in the direct dimension and 256 complex points in the indirect dimension in a linear fashion, with a subsequent 256 complex points being acquired with a non-uniform random sampling scheme. The total acquisition time for the indirect dimension was 113 ms. Sixty-four dummy scans were collected before the first increment, and 16 scans were acquired per increment.

The resulting HSQC spectra were processed using NMRPipe (see URLs). A zero order phase correction in the directly detected dimension was used. Spectra were then extracted in ascii format, and peaks from 0–10 ppm in the proton dimension and 20–160 ppm in the carbon dimension were considered. This resulted in 1,704 data points in the direct dimension and 423 data points in the indirectly detected dimension. The resulting intensities at each data point were then binned using an eightfold reduction in the proton dimension and a twofold reduction in the carbon dimension. The intensities at each point in the resulting 213 × 206 lattice were then computed, and a baseline value of 5×10^6 was defined that corresponded to a value above the signal-to-noise level; each bin with a sum intensity less than that of the baseline was set to the baseline. Bins in the region of the spectra containing the water line (4.60–4.75 ppm) were omitted. The resulting bins that had at least a twofold increase in the intensity relative to the noise level were considered. Individual metabolite assignments were carried out using the Human Metabolome Database (HMDB). Computer code was written in the PERL interpreting language. *z*-scores (intensities in standard units) were computed in MATLAB (see URLs). ^{13}C glycine peaks were integrated separately using the Sparky software package (see URLs). Peak intensities were computed using gaussian integration, and error bars were obtained from root mean square (RMS) residuals.

Targeted liquid-chromatography mass spectrometry (LC/MS/MS). We harvested 10^6 cells exponentially growing in basal media with dialyzed serum in 3 ml of 80% (v/v) methanol at dry ice temperatures. Fresh media was added 24 h and 2 h before the experiment. Insoluble material in lysates was centrifuged at 2,000*g* for 15 min, and the resulting supernatant was evaporated using a refrigerated speed vac. Samples were resuspended using 20 μl high performance liquid chromatography (HPLC)-grade water for mass spectrometry. We injected 10 μl and analyzed it using a 5500 QTRAP triple quadrupole mass spectrometer (AB/MDS Sciex) coupled to a Prominence ultra fast liquid chromatograph (UFLC) HPLC system (Shimadzu) using selected reaction monitoring (SRM) of a total of 249 endogenous water soluble metabolites for analyses of samples. Some metabolites were targeted in both the positive and negative ion mode for a total of 298 SRM transitions. ESI voltage was 5,000 V in the positive ion mode and −4,500 V in the negative ion mode. The dwell time was 5 ms per SRM transition, and the total cycle time was 2.09 s. Samples were delivered to the MS using normal phase chromatography using a 2.0 mm internal diameter × 15 cm Luna NH2 hydrophilic interaction chromatography (HILIC) column (Phenomenex) at 285 μl/min. Gradients were run starting from 85% buffer B (HPLC-grade acetonitrile) to 42% buffer B from 0–5 min; 42% buffer B to 0% buffer B from 5–16 min; 0% buffer B held from 16–24 min; 0% buffer B to 85% buffer B from 24–25 min; and 85% B held for 7 min to re-equilibrate the column. Buffer A was comprised of 20 mM ammonium hydroxide and 20 mM ammonium acetate in 95:5 water:acetonitrile. Peak areas from the total ion current for each metabolite SRM transition were integrated using MultiQuant v1.1 software (Applied Biosystems). Glucose-^{13}C–labeled samples were run with 249 total SRM transitions (40 transitions in positive ion mode and 209 in negative ion mode) with a total cycle time of 0.464 s.

Isotope labeling and kinetic profiling. Basal media using dialyzed serum without glucose was supplemented with [U^{13}C] glucose (Cambridge Isotope Laboratories) to a concentration equivalent to the concentration suggested by the ATCC protocol. Fresh media was added 2 h before the kinetics experiment. Media was replaced by equivalent [U^{13}C]-glucose–labeled media, and cells were quickly harvested at the given time points using the above mentioned protocol. Steady-state [U^{13}C]-glucose labeling involved labeling cells for 12 h before metabolite extraction. Samples were prepared as described above. Data analysis was performed in MATLAB.

Gas chromatography mass spectrometry (GC/MS). Cells were cultured in 6-well plates before replacing the medium with DMEM containing 10% dialyzed FBS and either [U-^{13}C] glucose plus unlabeled glutamine or [α-^{15}N] glutamine plus unlabeled glucose. After 24 h, cells were rinsed with

1 ml ice-cold PBS and quenched with 0.4 ml ice-cold methanol. An equal volume of water was added, and cells were collected in tubes by scraping with a pipette. One volume of ice-cold chloroform was added to each tube, and the extracts were vortexed at 4 °C for 30 min. Samples were centrifuged at 14,000*g* for 5 min, and the aqueous phase was transferred to a new tube for evaporation under nitrogen airflow. A two-step derivitization method was used as previously described[27]. Dried polar metabolites were dissolved in 20 µl of 2% methoxyamine hydrochloride in pyridine (Pierce) and held at 37 °C for 1.5 h. After dissolution and reaction, tert-butyldimethylsilyl (TBDMS) derivatization was initiated by adding 30 µl N-methyl-N- (tert-butyldimethylsilyl)trifluoroacetamide MBTSTFA plus 1% tert-butyldimethylchlorosilane TBDMCS (Pierce) and incubating at 55 °C for 60 min. GC/MS analysis was performed using an Agilent 6890 GC equipped with a 30 m DB-35MS capillary column connected to an Agilent 5975B MS operating under electron impact ionization at 70 eV. We injected 1 µl of sample in splitless mode at 270 °C using helium as the carrier gas at a flow rate of 1 ml/min. The GC oven temperature was held at 100 °C for 3 min and increased to 300 °C at 3.5°/min. The MS source and quadrupole were held at 230 °C and 150 °C, respectively, and the detector recorded ion abundances in the range of 100–600 m/z (mass to charge ratio). Mass isotopomer distributions for serine and glycine were determined by integrating ion fragments of 390–398 m/z and 246–252 m/z, respectively. Mass isotopomer distributions were corrected for natural isotope abundance using in house algorithms adapted from a previous study[28].

Analysis of somatic copy number alterations of *PHGDH*. Data were processed in MATLAB across 3,131 total samples and 150 melanoma samples from the Broad Institute as previously compiled[11]. Heatmaps were generated in MATLAB by first sorting copy number intensity at the coding region of *PHGDH*. False discovery rates (*q* values) on chromosome 1p were computed using a background model previously developed and plotted in MATLAB. *Q* values for candidate oncogenes were reported as in a previous study[11].

Cell proliferation assays. Lentiviral infection and puromycin selection were carried out under established protocols. After puromycin selection, control and knockdown cells were plated at equal densities and seeded cells were allowed to grow for three days before counting. Cell numbers were counted on the final day using an automated cell counter (Cellometer Auto T4, Nexcelom Bioscience) with custom morphological parameters set for each cell line. Error bars were reported using error propagation from the s.d. of three experiments.

Three-dimensional culture and confocal microscopy. To generate acini, cells were grown in reconstituted basement membrane (Matrigel) as described previously and according to established protocol (see URLs). The overlay media was changed every four days, and a given concentration of doxycycline (Sigma) was added where indicated. Acini were fixed between days 25 and 28, and immunofluorescence analyses of acini was performed as described previously. The following primary antibodies were used for immunofluorescence: cleaved caspase-3 (#9661, Cell Signaling Technology) and laminin-5 (mab19562, Millipore). The Golgi apparatus was detected by combining antibodies to the Golgi proteins GM130 (610823, BD Biosciences) and Golgin-84 (51-9001984, BD Biosciences). DAPI (Sigma-Aldrich) was used to counterstain nuclei. For examination of luminal filling, acini were imaged using confocal microscopy to visualize the center of each structure and then were scored as clear (~90–100% clear), mostly clear (~50–90% clear), mostly filled (~10–50% clear) or filled (~0–10% clear).

Fluorescence *in situ* hybridization (FISH). Cultured cell lines were harvested at 75% confluence, and metaphase chromosome spreads were produced using conventional cytogenetic methods. Human melanoma tissue arrays were first heated to remove paraffin. Slides were aged overnight at 37 °C, dehydrated by successive 2 min washes with 70%, 80%, 90% and 100% ethanol, air dried and then hybridized to DNA probes as described below. The following DNA probes were co-hybridized: RP11-22F13 (labeled in SpectrumGreen), which maps to 1p12 and includes *PHGDH*, and the D1Z5 alpha-satellite probe (SpectrumOrange, Abbott Molecular, Inc.), which maps to 1p11.1–q11.1. The RP11-22F13 BAC clone was obtained from CHORI (see URLs), direct labeled using nick translation and precipitated using standard protocols. The final probe concentration was 100 ng/µl. The tissue sections and probes were co-denatured at 80 °C for 5 min, hybridized for at least 16 h at 37 °C in a darkened humid chamber, washed in 2× saline-sodium citrate buffer (SSC) at 70 °C for 10 min, rinsed in room temperature (25 °C) 2× SSC and counterstained with DAPI (4′,6-diamidino-2-phenylindole; Abbott Molecular/Vysis, Inc.). Slides were imaged using an Olympus BX51 fluorescence microscope. Individual images were captured using an Applied Imaging system running CytoVision Genus version 3.92.

Human tumor samples and data analysis. Human breast cancer samples were obtained from the Harvard SPORE breast tissue repository collected under Dana-Farber/Harvard Cancer Center institutional review board protocol #93-085. Tumor and subject characteristics, tissue microarray construction and gene expression profiles were reported previously[29]. Histological diagnosis and comparison with clinical parameters was based on established criteria[29]. Human melanoma samples were obtained from the Yale SPORE skin cancer program and tissue microarray construction as previously reported[30]. Histological diagnosis was based on established criteria. All bioinformatics data from human breast cancer microarrays were obtained from Oncomine (see URLs) using established statistics[31].

27. Antoniewicz, M.R., Kelleher, J.K. & Stephanopoulos, G. Accurate assessment of amino acid mass isotopomer distributions for metabolic flux analysis. *Anal. Chem.* **79**, 7554–7559 (2007).
28. Fernandez, C.A., Des Rosiers, C., Previs, S.F., David, F. & Brunengraber, H. Correction of 13C mass isotopomer distributions for natural stable isotope abundance. *J. Mass Spectrom.* **31**, 255–262 (1996).
29. Richardson, A.L. *et al.* X chromosomal abnormalities in basal-like human breast cancer. *Cancer Cell* **9**, 121–132 (2006).
30. Hoek, K. *et al.* Expression profiling reveals novel pathways in the transformation of melanocytes to melanomas. *Cancer Res.* **64**, 5270–5282 (2004).
31. Rhodes, D.R. *et al.* ONCOMINE: a cancer microarray database and integrated data-mining platform. *Neoplasia* **6**, 1–6 (2004).

doi:10.1038/ng.890